Investigation of the electrical, optical and photophysical properties of PTB7:PCBM-thin films

Mohd Taukeer Khan[1,*] ⓘ

[1] *Department of Physics, Faculty of Science, Islamic University of Madinah, Madinah, Saudi Arabia*

ABSTRACT

Conjugated polymers offer flexible and lightweight solar cells devices which are fabricated via cost-effective solution processing techniques; however, these devices suffer from lower efficiency and short-term lifespan. To improve the efficiency and stability of device, the knowledge of the mechanism of the sun light absorption, dissociation of excitons into the free electron-hole pair and their transport to the collecting electrodes are essential. Herein, the impact of PCBM concentrations on photophysical and optical and properties of PTB7 were investigated by spectroscopic ellipsometer and fluorescence spectroscopy. It was noticed that with increase of PCBM concentrations, the dielectric constant (ε_r) and refractive index (n) of PTB7 thin films decreases which ascribed to the reduction of electric polarization and increase of the surface roughness. The emission intensity was noted to be dropped and charge carrier lifetime decreases for PTB7:PCBM bulkhetrojucntion as compared to pristine PTB7, confirms the charge transfer between donor and acceptor. The charge transport mechanism in PTB7 thin film was investigated in hole only device architecture by recording the temperature-dependent current-density vs. voltage (J–V) curves. The charge transport for the temperatures above 220 K was governed by the trap-free space charge limited (SCL) conduction described by Mott-Gurney square law and switched to the trap-filling SCL conduction for T ≤ 220 K. For the temperature 220 K, the trap density H_b, hole mobility μ and characteristics trap depth E_t were evaluated to be 2.98×10^{17} cm^{-3}, $\mu = 6.08 \times 10^{-5}$ cm^2 V^{-1} s^{-1} and 25 meV, respectively.

1 Introduction

Organic solar cells (OSC) is an emerging photovoltaic (PV) technology that offers the flexible, semitransparent, large-area and eco-friendly PV device [1–7]. Recently, the efficiency (η) of OSC has been improved and approaching towards the target value of 20% [8–13], however, it is still remains below the Si solar cells. Moreover, the long-term stability of OSC also poses a bottleneck in the commercialization of this technology. Various strategies including: encapsulation, interface engineering, solvent engineering, light trapping, photon management, material design, non-fullerene acceptors, optimization of device

Address correspondence to E-mail: khanmtk@iu.edu.sa

architecture, etc. have been employed to improve the device performance and lifetime of OSC [14–20]. At an early stage, poly(2-methoxy-5-(2-ethylhexyloxy)-1,4-phenylenevinylene) and thereafter poly(3-hexylthiophene) were the most common polymer used in combination with [6, 6]-phenyl-C_{61}-butyric acid methyl ester (PCBM), however, their performance remains ≤ 5% [21–23]. The low efficiency of OSC was primarily originated owing to the high exciton binding energy, low carrier mobility as well as short exciton diffusion length (10—20 nm). To solve this problem, the low band gap donor/acceptor (D/A) copolymers have been synthesized [24–30]. In a D/A copolymer, the photogenerated exciton quickly dissociated into the free electron and hole at the boundary of copolymer and accelerate the charge transport towards the respective electrodes.

Poly[(ethylhexyloxy)-benzodithiophene-(ethylhexyl)-thienothiophene] (PTB7) is a D/A copolymer with a band gap of 1.69 eV [31–39]. PTB7 in combination with $PC_{70}BM$ exhibits an efficiency over 9% [40]. Recently, Moiz et al. have simulated the solar cell performance PTB7:$PC_{70}BM$ using different electron transport layer (ETL) and proposed an efficiency of 17.15% with zinc oxysulfide as ETL [41]. The efficiency of PTB7:PCBM based bulkhetrojunction device could be further enhanced through the solvent-vapor and thermal annealing [42]. The morphology of the active layer was improved by using 5-hydroxy-2-methylpyrimidine as an additive, resulting in the substantially increased in the device performance as well as the thermal stability of device [43]. To further enhance the performance of PTB7:PCBM-based OSC, in depth knowledge of the electrical, photophysical as well as optical properties of the active layer is crucial.

The knowledge of the optical and photophysical properties of PTB7:PCBM-thin films can help in understanding the light absorption, exciton generation and dissociation into free electron and hole and their transport in device. By optimizing these aspects, the energy conversion efficiency of the OSC can be improved. Therefore, the effect of PCBM content on the photophysical and optical properties of PTB7 thin films was investigated by means of time-resolved fluorescence (TRF) spectroscopy and spectroscopic ellipsometer. These measurements provide the information about the optical constants including refractive index (n), dielectric constants (ε_r, ε_i), extinction coefficient (κ), energy band gap (E_g), charge carrier lifetime as well as the charge-transfer mechanism at

the D/A boundaries of the PTB7:PCBM. Moreover, with the variation in the PTB7:PCBM ratio, the optical and photophysical propoerties of active layer will also affect. Therfore, variation of optical properties with the different PTB7:PCBM wt. ratio were also investigated in order to optimize the weight ratio of D/A in active layer.

Besides the optical and photophysical properties, the performance of a device is greatly influence by the electrical parameters of the active layer. For example, the electrical resistivity and charge mobility of the polymer thin film can affect the efficiency of charge transport within the solar cell, which in turn affects the overall PCE of the device. Moreover, the conjugated polymers are characterized by the high trap density which are distributed spatially and energetically in the bandgap of semiconductor [44–47]. These traps act as non-radiative recombination centers where charge carrier get trapped and no longer participate in photocurrent generation process. Therefore, to further enhance the device performance of OSC, the knowledge of these electrical parameters including, charge carrier mobility, defect density, trap distribution and depth, activation energy and variation of the quasi-Fermi energy level with applied bias is essential. Herein, the electrical properties of PTB7 thin films were investigated in hole-only device configuration viz. indium tin oxide (ITO)/poly(3,4-ethylenedioxythiophene) polystyrene sulfonate (PEDOT:PSS) /PTB7/Au by recording the J–V characteristics at different temperatures. The experimental results were analyzed by the SCL conduction mechanism with traps distributted exponentially in space and important electrical parameters were evaluated.

2 Materials and methods

The ITO substrates were procured from Xin Yan Technology LTD which has the sheet resistance of 10 Ω/square. The PTB7 (PDI ≤ 3.0, Mw = 80,000–200,000) and PCBM were acquired through 1- Material inc. Poly(3,4-ethylenedioxythiophene)-poly(styrenesulfonate) (PEDOT:PSS) was purchased through Sigma Aldrich. Chlorobenzene (CB) and gold (Au) wire were acquired through Alfa-Aesar. The purchased chemicals and solvents were used without any treatment.

To record the optical and photophysical properties, the samples were prepared on glass substrates,

whereas the hole-only device for the electrical characterization was fabricated on ITO substrates. Before the start of sample fabrication, both glass and ITO substrates underwent a four steps cleaning process. First, they were treated with Hellmanex III (procured from Ossila), then rinsed with DI water, afterward immersed in acetone followed by methanol. The substrates were ultrasonicated for 15 min during each step. The cleaned substrates were dried with nitrogen gas and finally placed in plasma for 30 min to eliminate any remaining contaminants on their surfaces. The active layer solutions were made by 25 mg of PTB7 and PCBM in 1 mL of chlorobenzene (pH = 7) and allowed to be stirred for 12 h. Five solutions with different weight proportions of PTB7:PCBM (1:0, 1:0.5, 1:1, 1:1.5 and 1:2,) were prepared. These solutions were named PTB1:0, PTB1:0.5, PTB1:1, PTB1:1.5 and PTB1:2, corresponding to their weight proportions. To fabricate the hole transport layer, 100 μL of filtered (0.45 μm) PEDOT:PSS solution was dispensed on an ITO substrate and then spin-coated for 30 s at 5000 rpm. After that the samples were annealed for 10 min at 120 °C. Active layer was deposited inside the nitrogen-filled glove box by spin-casting the different PTB7:PCBM solutions at 2000 rpm for a period of 45 s, followed by annealing at 100 °C for 30 min. The fabricated PTB7/PCBM films were annealead for 30 min at 100 °C. Finally, top Au contact for SCLC measurements were applied using a thermal evaporation in a vacuum of 3×10^{-6} Torr.

The Delta-Flex TCSPC system fluorometer from Horiba (from Horiba) was employed to measure the steady state and time resolved decay spectra. A Delta-diode with a wavelength of $\lambda = 510 \pm 10$ nm was used to excite the samples and decay spectra was recorded at 765 nm. The optical properties of thin films were evaluated by Horiba Smart-SE spectroscopic Ellipsometer

in the wavelength region of 450–1050 nm. The spectroscopic data were analyzed by fitting the measured data with a software supplied by Horiba. The *J–V* characteristics at different temperatures were recorded from Keithley 4200 SCS and the device temperature was controlled by Linkam LTS420 heating/cooling stage. The *J–V* results were fitted with MathCAD software to extract the important electrical parameters.

3 Results and discussion

3.1 Photophysical properties

To better understand how PCBM concentration affects the photophysical properties of PTB7, the steady-state and TRF spectra of PTB7: PCBM were measured which are shown in Fig. 1a and b respectively. The maxima of PL spectra was noted around at 753 nm, which is attributed to the decay of excitons from the excited state to the ground state [48, 49]. The PL intensity found to be fully quenched for PTB7:PCBM films even for the lowest concentration of PCBM. The decrease in PL intensity in PTB7:PCBM-thin films is corresponds to the transfer of electron from PTB7 to the PCBM [50, 51]. In other words, the photoexcited exciton dissociates at the interface of PTB7/PCBM and the electron transfers to the PCBM while the hole remains in PTB7 [52]. It can be noticed from TRF decay spectra shown in Fig. 1b that the PCBM accelerates the decay in PTB7, attributed to the faster exciton diffusion in the presence of acceptor PCBM. The TRF spectra was fitted with the bi-exponential decay function [53–55]:

$$I(t) = B_0 + B_1 e^{-t/\tau_1} + B_2 e^{-t/\tau_2} \tag{1}$$

where the time constant τ_1 corresponds to charge transfer at the PTB7/PCBM interface and time constant

Fig. 1 **a** The steady-state PL and **b** time-resolved fluorescence spectra of fabricated PTB7:PCBM-thin films.
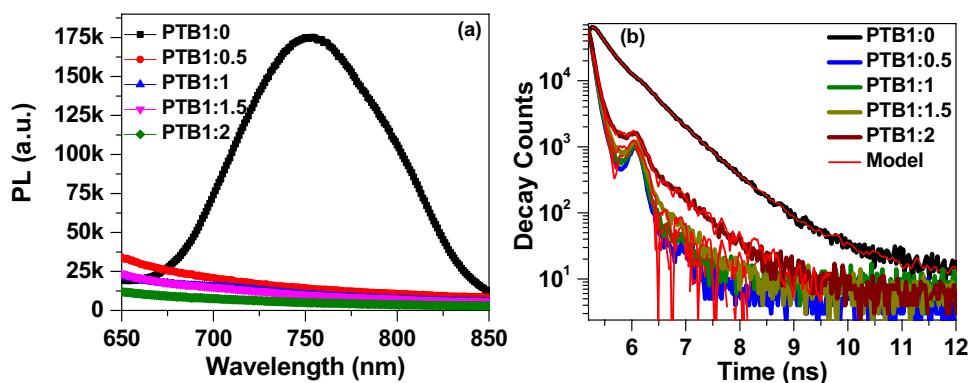
τ_2 is related to the lifetime of exciton in PTB7 bulk [56], B_0, B_1, and B_2 are the fitting constants, which are listed in Table 1. It can be noticed that the lifetime τ_1 decreases, indicating the exciton dissociation and faster charge transport across PTB7/PCBM interface. On the contrary, the lifetime τ_2 increases, suggesting longer living charge carriers in PTB7 bulk. Furthermore, the sample PTB1:1.5 has the shortest value of τ_1, confirming the fastest charge transfer for this D/A combination. Moreover, for the PTB7:PCBM concentrations 1:0.5 the decay is faster due to increase of defect density in active layer, however, the decay is slowing down with increase of concentration indicating the charge transfer from PTB7 to PCBM.

3.2 Optical properties

The spectroscopic ellipsometer is a surface-sensitive, non-destructive technique extensively employed to study the optical properties of thin films. The measurement of spectroscopic ellipsometer provide the optical parameters constants including: n, κ, ε_r, ε_i, optical band gap (E_g) surface roughness (r) as well as the thickness of thin film (d). The optical parameters are determined by measuring the change in amplitude (ψ) and phase shift (Δ) of incident light upon reflection from film surface. The measured data were theoretically fitted with the New-Amorphous Dispersion formula given by: [57–60]**:**

$$n(\omega) = n_\infty + \sum_{j=1}^{2} \frac{B \cdot \left(\omega - \omega_j\right) + C}{\left(\omega - \omega_j\right)^2 + \Gamma_j^2} \quad (2)$$

$$k(\omega) = \begin{cases} \sum_{j=1}^{2} \frac{f_j \cdot \left(\omega - \omega_g\right)^2}{\left(\omega - \omega_j\right)^2 \cdot \Gamma_j^2}, & \omega > \omega_g \\ 0, & \omega \leqslant \omega_g \end{cases} \quad (3)$$

where $B = \frac{f_i}{\Gamma_j} \cdot \left(\Gamma_j^2 - \left(\omega_j - \omega_g\right)^2\right)$, $C = 2 \cdot f_i \cdot \Gamma_j \cdot \left(\omega_j - \omega_g\right)$ and n_∞ is the high frequency refractive index.

The fitting of experimental data was carried out using the effective medium approximation (EMA) optical model shown in Fig. 2a [61]. The experimental data exhibits a good fitting with the theoretical model as illustrated by solid lines in Fig. 2b. Moreover, the curve fitting constant $\chi^2 < 2$ further confirms the validity of this model. The parameters extracted from the fitting of the experimental ellipsometer data are listed in Table 2. Film thickness of pure PTB7 was found to be ≈ 117 nm with a roughness of 6 nm. Moreoever, the film thickness gradually decrease with increase of PCBM content while roughness of hybrid films were noted to be slightly higher with a value of ~ 10 nm.

Figure 3a–d illustrates how optical constants vary with respect to the wavelength of light. The peak value of the n for pure PTB7 was observed $n_{max} = 2.33$ around

Table 1 The TRF decay fit parameters of PTB7:PCBM thin films

Film	τ_1 (ps)	B_1%	τ_2 (ps)	B_2%	τ_{avg} (ps)	χ^2
PTB1:0	256	2	35	98	153	1.15
PTB1:0.5	177	34	39	66	122	1.80
PTB1:1	143	54	98	46	126	1.54
PTB1:1.5	71	49	72	51	71	1.13
PTB1:2	23	70	135	30	103	1.87

Fig. 2 a The optical model that was employed to fit the measured data **b** (symbol) The ratio of amplitude change (ψ) and phase shift (Δ) of PTB7 thin film. (Solid line) theoretically generated curve using new amorphous dispersion model.
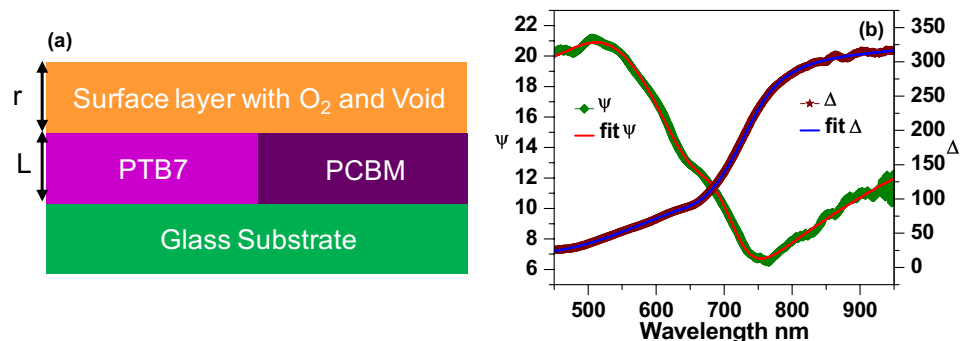
Table 2 Optical parameters evaluated from the fitting of the experimental spectroscopic Ellipsometer data

Sample	PTB1:0	PTB1:0.5	PTB1:1	PTB1:1.5	PTB1:2
d (nm)	117	117	106	103	101
r (nm)	6	10	10	10	10
E_g (eV)	1.69	1.87	1.95	2.02	2.08
n_{max}	2.33	2.19	2.05	1.68	1.56
κ_{max}	0.86	0.80	0.76	0.51	0.48
$\varepsilon_{r,max}$	4.28	3.94	3.76	3.32	3.10
$\varepsilon_{i,max}$	2.91	2.52	2.03	1.80	1.39
χ^2	1.4	1.34	1.10	1.95	1.79

713 nm, which is similar to that of the P3HT [60]. The refractive index found to be gradually decreases as the concentration of PCBM increases in PTB7. The peak refractive index of PTB1:0.5, PTB1:1, PTB1:1.5 and PTB1:2 was noted to be 2.19, 2.05, 1.68 and 1.56, respectively. The decrease in the value of n with PCBM corresponds to the drop in the polarization of films due to charge transfer between PTB7 and PCBM as well as the increase of surface roughness as presented in Table 2. Moreover, with the increase of PCBM content, the charge carrier concentration (n_c) increases,

consequently decrease in the value of refractive index n could be explained through the formula [62]:

$$n^2 = \varepsilon_{opt} - \left(\frac{4\pi n_C e^2}{m * \omega_0^2} \right) \tag{4}$$

where ω_0 is the frequency of incident light, ε_{opt} is the optical permittivity, e and m* are the charge and effective mass of the electron, respectively. On incorporation of PCBM in PTB7 film, the excitons dissociate at the D/A boundaries, creating free electrons and holes, consequently, n_c increases while refractive index decreases.

The optical bandgap of pristine PTB7 was evaluated to be 1.69 eV which is higher than the 1.60 eV [63], 1.64 eV [64], and close to the 1.70 eV [65] of the reported values. The band gap was found to be higher for hybrid PTB7:PCBM film as compared to pristine films. The increase in the band gap with the PCBM content can be explained through the decrease in the value of n. As n decreases, the density of states (DOS) around the top of the valence band (VB) and bottom of conduction bands (CB) decreases, leading to an increase in the energy required to excite an electron from the top of VB to the bottom of the CB, as a result optical bandgap increases [66, 67].

Fig. 3 The variation of optical parameters **a** n, **b** κ, **c** ε$_r$ and, **d** ε$_i$.
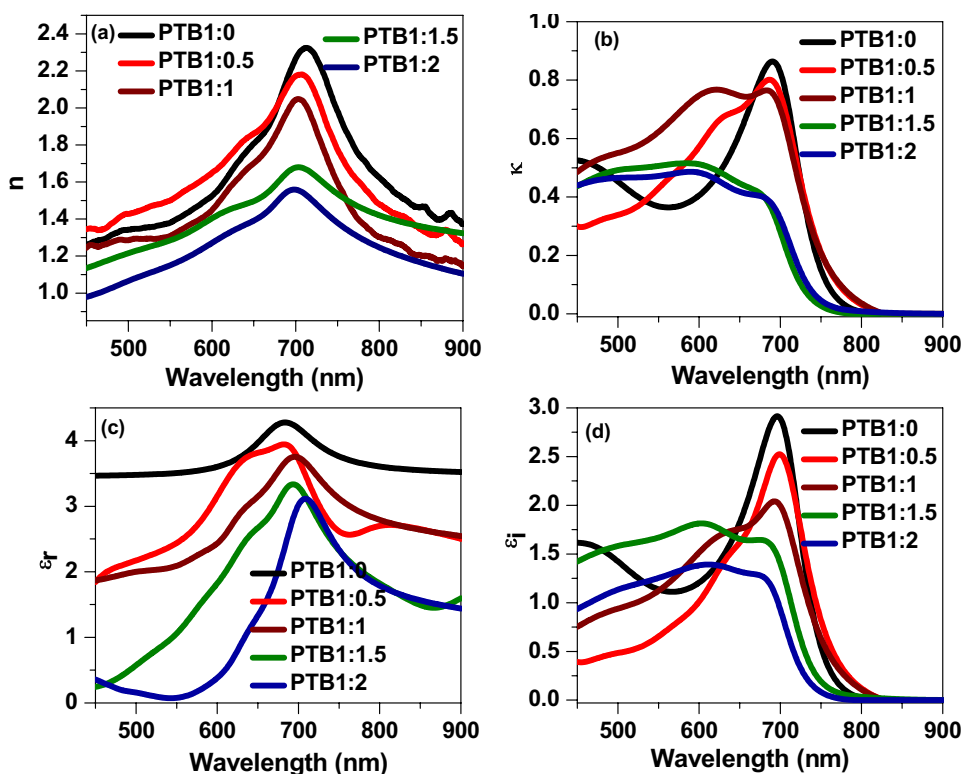
The variation of the κ as a function of the wavelength of pure PTB7 and PTB7:PCBM hybrid thin films are displayed in Fig. 3b. The extinction coefficient reflect the optical energy loss inside the material which found to be decrease with the increase of PCBM content in thin films. The pure PTB7 films exhibits a peak value of κ_{max} ~ 0.86 which drops to 0.48 for the PTB1:2 film (Table 2). The decrease in κ can be explained through the low absorption coefficient of PCBM as compared to PTB7. With the increase of PCBM quantity, the absorption coefficient of hybrid film decreases as a result the value of κ decreases. The variation of ε_r and ε_i with wavelength are shown in Fig. 3c, and d, respectively. The peak of the ε_r and ε_i of pure PTB7 thin film was observed ~ 682 nm with a value of $\varepsilon_{r,max}$ ~ 4.28. The dielectric constant was found to be almost constant on both sides of the peak with a value in the range of 3.4–3.5. Moreover, the ε_r of the PTB7 thin films was found to be decrease gradually with the increase of the PCBM concentrations. The peak value of the dielectric constant were noted to be 3.94, 3.76, 3.32, and 3.10 for the samples PTB1:0, PTB1:0.5, PTB1:1, PTB1:1.5 and PTB1:2, respectively. The lower value of ε_r in hybrid PTB7:PCBM-thin films indicates that photogenerated excitons dissociate faster than in pure PTB7, as confirmed by the shorter value of τ_1 in Table 1. The dissociation of exciton into the free charge carriers causes decrease the electric polarization, consequently, decrease of dielectric constant. Moreover, the increase of surface roughness also cause for the decrease of dielectric constant. The constant ε_i reflect the dissipation of the electrical energy within the material. It can be noticed from Fig. 3d

that ε_i exhibits a similar pattern as the extinction coefficient. The peak value of ε_i for the pristine PTB7 was recorded around at 690 nm with $\varepsilon_{i,max}$ = 2.91. The ε_i was also found to decrease with increase of PCBM amount. The with peak values of of ε_i was evaluated to be 2.52, 2.03, 1.80, and 1.39 for the samples PTB1:0, PTB1:0.5, PTB1:1, PTB1:1.5 and PTB1:2, respectively.

3.3 Electrical properties

In order to reveals the charge transport mechanism and evaluate the important electrical parameters, the J–V characteristics of PTB7 were recorded at different temperature in the hole-only device architecture of ITO/PEDOT:PSS/PTB7/Au as shown in the inset of Fig. 4b. It can be noticed from Fig. 4a and b that the J–V characteristics exhibit different behaviors at low and high temperatures. The Fig. 4a displays that the J-V characteristics at low temperatures (T ≤ 220 K) have three distinct regions: A, B and C with corresponding slopes of one, greater than two and two, respectively. For a small bias (region A), the injected carrier density (ρ) is very small compared to thermally generated charge density (ρ_0) and mathematically expressed through the inequality [68]:

$$qp_0\mu\frac{V}{d} > \frac{9}{8}\varepsilon_0\varepsilon_r\mu\frac{V^2}{d^3} \qquad (5)$$

where q is the fundamental charge, μ is the hole mobility, ε_0 is the permittivity of free space, ε_r is the dielectric constant of material. The injected carrier density gradually increases with applied bias and when injected carrier density becomes equal to the density
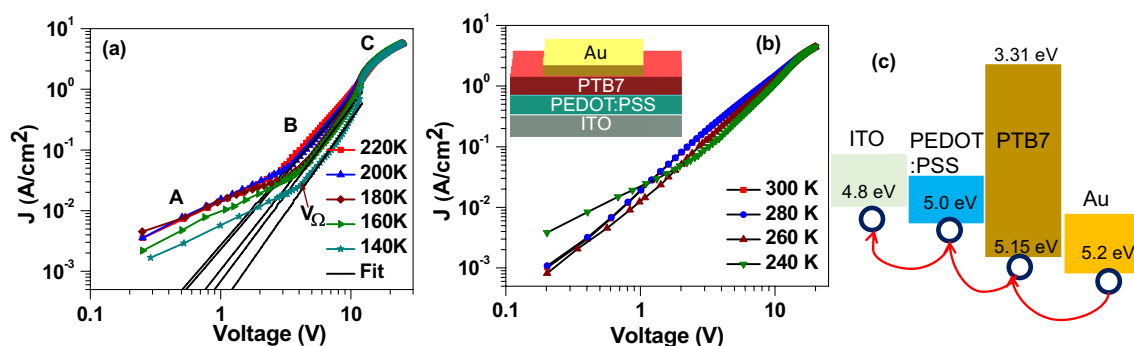

Fig. 4 *J-V* characteristics of PTB7 based hole only device for the temperature range **a** 220 K—140 K and **b** 300 K—240 K. Experimental (symbols) and fitted (solid lines). Inset (b) shows the device schematics. **c** Schematic illustration of energy band diagram of hole-only device.

of thermally generated carrier, the conduction mechanism switch to trap-limited SCLC (region B) at a voltage given by Equation [68]:

$$V_\Omega = \frac{qd^2H_b}{\varepsilon_0\varepsilon_r}\left(\frac{p_0}{N_{\text{HOMO}}}\right)^{1/l}\left(\frac{l+1}{l}\right)\left(\frac{l+1}{2l+1}\right)^{l+1/l} \tag{6}$$

where H_b is the total density of traps, N_{HOMO} is the effective density of traps at the edge of the highest occupied molecular orbital (HOMO) level. The current in the trap-limited SCLC region follows the Equation:

$$J = q^{1-l}\mu N_{\text{HOMO}}\left(\frac{2l+1}{l+1}\right)^{l+1}\left(\frac{l}{l+1}\frac{\varepsilon_r\varepsilon_0}{H_b}\right)^l\frac{V^{l+1}}{d^{2l+1}} \tag{7}$$

where $l = E_t/k_BT$ with $E_t = k_BT_C$ is the characteristic trap energy and T_C is the characteristics temperature of trap distribution. The E_t is a crucial parameter, signifying the quality of the thin film and it is the energy level where trap density of drops to 1/e compared to the edge of HOMO level [46].

It can be noticed from Fig. 4a that the theoretically generated curves using Eq. 7 (solid black lines) exhibit good fitting to the experimentally measured J–V curve in region B. The parameters used to fit the trap-limited SCLC region at 220 K are; $H_b = 2.98 \times 10^{17}~cm^{-3}$, $N_{HOMO} = 2.0 \times 10^{17}~cm^{-3}$, $\varepsilon_r = 3.4$, $\varepsilon_0 = 8.85 \times 10^{-14}~F/cm$, $\mu = 5.9 \times 10^{-5}~cm^2~V^{-1}~s^{-1}$, $d = 120~nm$, and $T_c = 290~K$, corresponds to $E_t \sim 25~meV$. The value of characteristics trap energy in PTB7 is small as compared to 45 meV for P3HT [69, 70] and 86 meV for PCDTBT [46]. The low value of characteristics trap energy indicates that room temperature thermal energy is enough to discharge the trapped charge.

With increase of applied bias, the density of injected carriers increases. Owing to the poor charge carrier mobility of organic semiconductors, the additional charge carriers cannot transport to the collecting electrode at the same rate at which they were being injected. These extra injected carriers start occupying the trap states, consequently the rate of the increase of current with applied bias decreases. As the applied bias increases and reaches the crossover voltage V_C, the J–V curve deviates from trap-limited SCLC, and the slope reduces to 2 (region C). The change in the conduction mechanism from trap-limited SCL to trap-free SCL was observed within a small range of crossover voltage

$V_C \sim 13.20~V - 14.90~V$, which is given through the Equation:

$$V = V_C = f(l)\frac{qd^2H_b}{\varepsilon\varepsilon_0} \tag{8}$$

where,

$$f(l) = \left(\frac{2l+1}{l+1}\right)^{-1/l}\frac{(l+1)^2}{l(2l+1)} \tag{9}$$

At crossover voltage, all the trap states are occupied by injected carriers and the transport mechanism in PTB7 thin film change from trap-filling SCLC conduction to trap-free SCLC conduction which is describes by the Mott-Gurney square law:

$$J = \frac{9}{8}\varepsilon_0\varepsilon_r\mu\frac{V^2}{d^3} \tag{10}$$

Moreover, the current in region C is independent of temperature, however, in region B, current increases with the temperature as illustrated in Fig. 5a. The total trap density H_b at different temperature was evaluated using Eq. 8 and Eq. 9 which are presented in Table 3. It can be noticed from Table 3 shows that with the increase of temperature the trap density decrease, indicating occupation of traps states by charge carriers that are thermally generated. The hole mobility in region C was evaluated to be $6.08 \times 10^{-5}~cm^2/Vs$ and remains constant with temperature. Figure 4b shows that the J–V characteristics in region B deviate from Eq. 7 for temperatures higher than 220 K and follow the Mott-Gurney square law. As discussed above that the density of thermally generated charge carriers increases with temperature. Thermally generated carriers start occupying the trap states, consequently trap density decreases with the temperature. Hence, charge transport in PTB7 film exhibits trap-limited SCLC for the temperature ≤ 220 K and switches to the trap-free SCLC for the higher temperature. The variation of mobility in region B as a function of temperature is illustrated in Fig. 5b, also the same listed in Table 3. The mobility was found to be temperature-dependent and increases exponentially with temperature. The room temperature SCLC mobility of PTB7 was evaluated to be $6.08 \times 10^{-5}~cm^2/Vs$, which is about one order higher than P3HT ($1.4 \times 10^{-5}~cm^2/Vs$) [69, 70] and PCDTBT ($2.42 \times 10^{-5}~cm^2/Vs$) [46]. A comparison of the electrical and optical parameters of PTB7, P3HT and PCDTBT thin films are presented in Table 4.

Fig. 5 **a** log(J) vs. 1000/T plots at different applied biases. **b** Variation of SCLC hole mobility as a function of temperature.
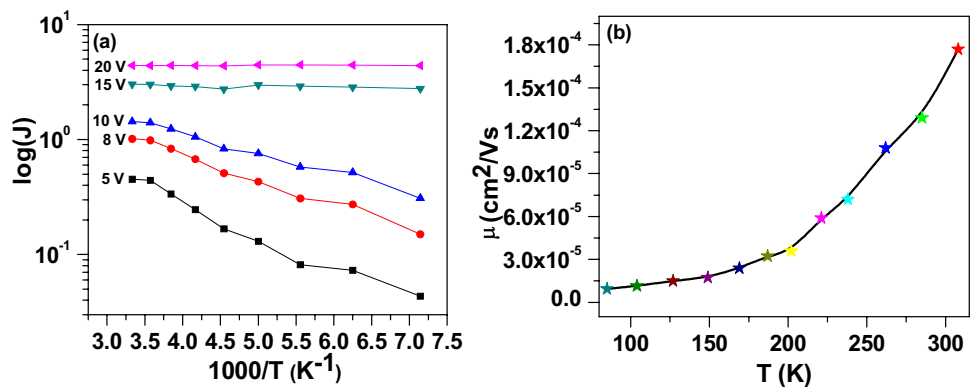

Table 3 Electrical parameters of PTB7 thin film at different temperatures evaluated from the *J-V* characteristics

T (K)	H_b (cm^{-3})	μ (cm^2/Vs)	E_t (meV)
140	4.19×10^{17}	1.74×10^{-5}	45
160	3.77×10^{17}	2.39×10^{-5}	37
180	3.71×10^{17}	3.23×10^{-5}	35
200	3.20×10^{17}	3.59×10^{-5}	28
220	2.98×10^{17}	5.9×10^{-5}	25
240	2.69×10^{17}	7.2×10^{-5}	24

energy level coincides for all temperatures, indicating the filling of all trap states. Moreover, when applied bias, the quasi-Fermi energy level becomes zero i.e., $E_{F,p}$ coincides with HOMO level. Additionally, for the applied bias less than V_C, the $E_{F,p}$ decreases with the temperature, however, for $V > V_C$, it increases with temperature, attributed to two different conduction mechanisms in PTB7 thin films, i.e., trap-limited SCLC fwor $V \leq V_C$ and trap-free SCLC for $V > V_C$.
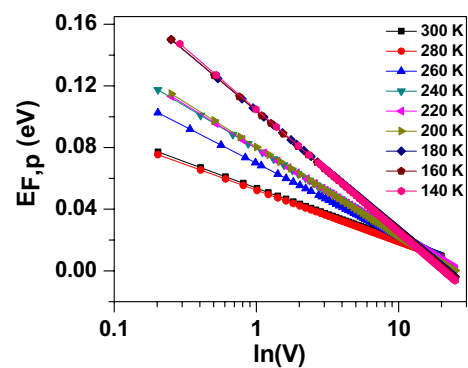
Furthermore, as discussed above, the charge carrier density inside the PTB7 films depends on applied bias and temperature. As the charge carrier density increases due to the applied bias and temperature, the quasi-Fermi level for the hole ($E_{F,p}$) decreases. The relationship between the quasi-Fermi level and the applied bias is expressed by Equation: [71, 75]

$$E_{F,p}(V) = k_B T_C \ln \left[f(l) \frac{q d^2 H_b}{\varepsilon \varepsilon_0 V} \right] \tag{11}$$

The quasi-Fermi level was evaluated by substituting the value of H_b in Eq. 11 and illustrated as a function of applied bias in Fig. 6. Figure 6 shows that the $E_{F,p}$ linearly decreases with the ln(V) $E_{F,P}$ level at temcoincides and at crossover voltage V_C, the quasi-Fermi

Fig. 6 Variation of quasi-Fermi level as a function of applied bias and device temperature.

Table 4 Comparison of optical and electrical parameters of PTB7, PCDTBT and P3HT thin films

Parameter/ Material	Eg (eV)	n	ε_∞	μ (cm^2 V^{-1} s^{-1})	E_t (meV)	H_b (cm^{-3})
PTB7	1.69	2.33	3.23 [72]	6.08×10^{-5}	25	2.98×10^{17}
PCDTBT	1.90 [73]	2.45 [74]	3.6 [74]	2.42×10^{-5} [46]	86 [46]	1.28×10^{17} [46]
P3HT	1.92 [60]	2.30 [60]	3.08 [60]	1.40×10^{-5} [69]	45 [69]	1.50×10^{17} [69]

4 Conclusions

In conclusions, the different PTB7:PCBM compositions were investigated. The κ optical constants (n, κ, ε_r, ε_i) were found to be decreases with the increase of PCBM concentrations. The PL quenching and faster fluorescence decay with the increase of PCBM concentration indicates the charge separation at PTB7/PCBM interface. The charge transport in PTB7 thin film was investigated in hole-only device and found to be governed by the Mott-Gurney square law for T > 200 K which and switched to the trap-filling SCL conduction at low temperatures. The trap density H_b, hole mobility μ and characteristics trap depth E_t in PTB7 films were evaluated to be *4.19 × 10^{17} cm^{-3}, 6.08 × 10^{-5} cm^{2}V^{-1}s^{-1}, and 25 meV,* respectively.

Acknowledgements

Funding

Data availability

The data that support the findings of this study are available from the corresponding author upon reasonable request.

Declarations

Conflict of interest The authors have no conflicts to disclose.

References

1. S.B. Mdluli, M.E. Ramoroka, S.T. Yussuf, K.D. Modibane, V.S. John-Denk, E.I. Iwuoha, π-conjugated polymers and their application in organic and hybrid organic-silicon solar cells. Polymers **14**(4), 716 (2022)

2. P. Xue, P. Cheng, R.P.S. Han, X. Zhan, Printing fabrication of large-area non-fullerene organic solar cells. Mater. Horiz. **9**, 194–219 (2022)

3. C. Liao, Y. Gong, X. Xu, L. Yu, R. Li, Q. Peng, Cost-Efficiency balanced polymer acceptors based on lowly fused Dithienopyrrolo[3, 2b]benzothiadiazole for 16.04% efficiency All-Polymer solar cells. Chem. Eng. J. **435**, 134862 (2022)

4. F. Yang, Y. Huang, Y. Li, Y. Li, Large-area flexible organic solar cells. npj Flex. Electron. **5**, 30 (2021)

5. X. Kong, J. Zhang, L. Meng, C. Sun, X. Jiang, J. Zhang, C. Zhu, G. Sun, J. Li, X. Li, Z. Wei, Y. Li, Low-cost and high-performance polymer solar cells with efficiency insensitive to active-layer thickness. CCS Chem. (2023). https://doi.org/10.31635/ccschem.023.202302720

6. B. Liu, H. Sun, J.W. Lee et al., Efficient and stable organic solar cells enabled by multicomponent photoactive layer based on one-pot polymerization. Nat. Commun. **14**, 967 (2023)

7. H. Yu, Y. Wang, X. Zou et al., Improved photovoltaic performance and robustness of all-polymer solar cells enabled by a polyfullerene guest acceptor. Nat. Commun. **14**, 2323 (2023)

8. L. Liu, S. Chen, Y. Qu, X. Gao, L. Han, Z. Lin, L. Yang, W. Wang, N. Zheng, Y. Liang, Y. Tan, H. Xia, F. He, Nanographene-osmapentalyne complexes as a cathode interlayer in organic solar cells enhance efficiency over 18%. Adv. Mater. **33**, 2101279 (2021)

9. M.A. Green, E.D. Dunlop, J. Hohl-Ebinger, M. Yoshita, N. Kopidakis, K. Bothe, D. Hinken, M. Rauer, X. Hao, Solar cell efficiency tables (Version 60). Prog Photovolt Res Appl. **30**, 687–701 (2022)

10. L. Zhu, M. Zhang, J. Xu et al., Single-junction organic solar cells with over 19% efficiency enabled by a refined double-fibril network morphology. Nat. Mater. **21**, 656–663 (2022)

11. R. Sun, Y. Wu, X. Yang, Y. Gao, Z. Chen, K. Li, J. Qiao, T. Wang, J. Guo, C. Liu, X. Hao, H. Zhu, J. Min, Single-junction organic solar cells with 19.17% efficiency enabled by introducing one asymmetric guest acceptor. Adv. Mater. **34**(26), 2110147 (2022)

12. L. Zhou, L. Meng, J. Zhang, C. Zhu, S. Qin, I. Angunawela, Y. Wan, H. Ade, Y. Li, Introducing Low-cost pyrazine unit into terpolymer enables high-performance polymer solar cells with efficiency of 18.23%. Adv. Funct. Mater. **32**(8), 2109271 (2022)

13. Fu. Jiehao, P.W.K. Fong, H. Liu, C.-S. Huang, Lu. Xinhui, Lu. Shirong, M. Abdelsamie, T. Kodalle, C.M. Sutter-Fella, Y. Yang, G. Li, 19.31%binary organic solar cell and low

non-radiative recombination enabled by non-monotonic intermediate state transition. Nat. Commun. (2023). https://doi.org/10.1038/s41467-023-37526-5

14. W. Lan, J. Gu, S. Wu, Y. Peng, M. Zhao, Y. Liao, T. Xu, B. Wei, L. Ding, F. Zhu, Toward improved stability of non-fullerene organic solar cells: impact of interlayer and built-in potential. EcoMat. **3**(5), e12134 (2021)

15. L.J.F. Hart, J. Grüne, W. Liu, T.-k Lau, J. Luke, Y.-C. Chin, X. Jiang, H. Zhang, D.J.C. Sowood, D.M.L. Unson, J.-S. Kim, Lu. Xinhui, Y. Zou, F. Gao, A. Sperlich, V. Dyakonov, J. Yuan, A.J. Gillett, Understanding the Role of triplet-triplet annihilation in non-fullerene acceptor organic solar cells. Adv. Energy Mater. **13**, 2301357 (2023)

16. L. Di Mario, D.G. Romero, M.J. Pieters, F. Eller, C. Zhu, G. Bongiovanni, E.M. Herzig, A. Murad, M.A. Loi, Effects of the diphenyl ether additive in halogen-free processed non-fullerene acceptor organic solar cells. J. Mater. Chem. A **11**, 2419 (2023)

17. P. Gattu Subramanyam, N. Krishnaswamy, K. Guha, J. Iannacci, E.N. Ude, V. Muniswamy, Enhanced optical management in organic solar cells by virtue of square-lattice triple core-shell nanostructures. Micromachines **14**, 1574 (2023)

18. C. Zhao, R. Ma, Y. Hou, L. Zhu, X. Zou, W. Xiong, Hu. Huawei, L. Wang, Yu. Han, Y. Wang, G. Zhang, Lu. Jicheng Yi, D.W. Chen, T. Yang, G. Li, M. Qiu, He. Yan, S. Li, G. Zhang, 18.1% Ternary All-polymer solar cells sequentially processed from hydrocarbon solvent with enhanced stability. Adv. Energy Mater. **13**, 2300904 (2023)

19. H. Tang, Y. Bai, H. Zhao, X. Qin, Hu. Zhicheng, C. Zhou, F. Huang, Y. Cao, Interface Engineering for highly efficient organic solar cells. Adv. Mater. (2023). https://doi.org/10.1002/adma.202212236

20. L. Meng, H. Liang, G. Song et al., Tandem organic solar cells with efficiency over 19% via the careful subcell design and optimization. Sci. China Chem. **66**, 808–815 (2023)

21. S.E. Shaheen, C.J. Brabec, N.S. Sariciftci, F. Padinger, T. Fromherz, J.C. Hummelen, The 2.5% efficient organic plastic solar cells. App. Phys. Lett. **78**(6), 841–843 (2001)

22. M. Reyes-Reyes, K. Kim, D.L. Carroll, High-efficiency photovoltaic devices based on annealed poly(3-hexylthiophene) and 1-(3-methoxycarbonyl)-propyl-1- phenyl-(6,6) C61 blends. Appl. Phys. Lett. **87**, 083506 (2005)

23. M.T. Khan, M. Shkir, A. Almohammedi, Fabrication Methods of Thin Film Polymer Solar Cells, in *Nanomaterials for Optoelectronic Applications*. ed. by M. Shkir, A. Kaushik, S. Alfaifi (Publisher Apple Academic press, Boca Raton, 2021), pp.201–232

24. M. Sommer, S. Huettnerab, M. Thelakkat, Donor–acceptor block copolymers for photovoltaic applications. J. Mater. Chem. **20**, 10788–10797 (2010)

25. H. Zhou, L. Yang, S. Stoneking, W. You, A weak donor–strong acceptor strategy to design ideal polymers for organic solar cells. ACS Appl. Mater. Interfaces **2**(5), 1377–1383 (2010)

26. H. Xin, X. Guo, F.S. Kim, G. Ren, M.D. Watson, S.A. Jenekhe, Efficient solar cells based on a new phthalimide-based donor–acceptor copolymer semiconductor: morphology, charge-transport, and photovoltaic properties. J. Mater. Chem. **19**, 5303–5310 (2009)

27. N.M. Ahmed, Alahmadi, design of an efficient PTB7:PC70BM-based polymer solar cell for 8% efficiency. Polymers **14**, 889 (2022)

28. C. Sun, C. Zhu, L. Meng, Y. Li, Quinoxaline-based D-A copolymers for the applications as polymer donor and hole transport material in polymer/perovskite solar cells. Adv. Mater. **34**(22), 2104161 (2022)

29. M.L. Keshtov, I.O. Konstantinov, A.R. Khokhlov, I.E. Ostapov, V.G. Alekseev, Z. Xie, H. Dahiya, G.D. Sharma, Synthesis of D-A copolymers based on thiadiazole and thiazolothiazole acceptor units and their applications in ternary polymer solar cells. J. Polym. Sci. **60**(14), 2086–2099 (2022)

30. L. Li, F. Meng, M. Zhang, Z.-G. Zhang, D. Zhao, Revisiting the dithienophthalimide building block: improved synthetic method yielding new high-performance polymer donors for organic solar cells. Angew. Chem. **134**(35), e202206311 (2022)

31. Y.-C. Chao, J.-H. Chen, Y.-J. Chiou, P.-L. Kao, J.-L. Wu, C.-T. Chen, L.-H. Chan, R.-J. Jeng, Design of thienothiophene-based copolymers with various side chain-end groups for efficient polymer solar cells. Polymers **12**, 2964 (2020)

32. L. Lu, L. Yu, Understanding low bandgap polymer PTB7 and optimizing polymer solar cells based on it. Adv. Mater. **26**(26), 4413–4430 (2014)

33. L. Lu, T. Zheng, T. Xu, D. Zhao, L. Yu, Mechanistic studies of effect of dispersity on the photovoltaic performance of PTB7 polymer solar cells. Chem. Mater. **27**(2), 537–543 (2015)

34. Y. Du, Y. Li, O. Aftenieva, T. Tsuda, P. Formanek, T.A.F. König, A. Synytska, High yield synthesis of water-processable donor: acceptor janus nanoparticles with tuned internal morphology and highly efficient charge separation/transfer. Adv. Opt. Mater. **10**, 2101922 (2022)

35. S. Foster, F. Deledalle, A. Mitani, T. Kimura, K.-B. Kim, T. Okachi, T. Kirchartz, J. Oguma, K. Miyake, J.R. Durrant, S. Doi, J. Nelson, Electron collection as a limit to polymer:PCBM solar cell efficiency: effect of blend microstructure on carrier mobility and device performance in PTB7:PCBM. Adv. Energy Mater. **4**, 1400311 (2014)

36. N. Kleinhenz, L. Yang, H. Zhou, S.C. Price, W. You, Low-band-gap polymers that utilize quinoid resonance structure stabilization by thienothiophene: fine-tuning of HOMO level. Macromolecules **44**(4), 872–877 (2011)

37. Y. Gao, M. Liu, Y. Zhang, Z. Liu, Y. Yang, L. Zhao, Recent development on narrow bandgap conjugated polymers for polymer solar cells. Polymers **9**(2), 39 (2017)

38. E. Çokduygulular, Ç. Çetinkaya, S. Emik et al., In-depth analysis on PTB7 based semi-transparent solar cell employing MoO_3/Ag/WO_3 contact for advanced optical performance and light utilization. Sci. Rep. **13**, 7548 (2023)

39. W. Sung, H. Lee, W. Choi et al., Nanomorphology dependence of the environmental stability of organic solar cells. NPG Asia Mater. **14**, 56 (2022)

40. Z. He, C. Zhong, S. Su, M. Xu, H. Wu, Y. Cao, Enhanced power-conversion efficiency in polymer solar cells using an inverted device structure. Nat. Photon. **6**(9), 591–595 (2012)

41. S.A. Moiz, M.S. Alzahrani, A.N.M. Alahmadi, Electron transport layer optimization for efficient PTB7:PC70BM Bulk-heterojunction solar cells. Polymers **14**, 3610 (2022)

42. X. Zhang, J. Wang, Z. Li et al., Improved photovoltaic performance of PTB7:PC71BM blend by thermal annealing and solvent vapor annealing. Colloid Polym. Sci. **301**, 11–18 (2023)

43. Q. Zhang, C. Bao, S. Cui, P. Zhong, K. Zhang, W. Zhu, Yu. Liu, Boosting the efficiency of PTB7-Th:PC71BM polymer solar cells via a low-cost halogen-free supramolecular solid additive. J. Mater. Chem. C **8**, 16551–16560 (2020)

44. M.T. Khan, V. Agrawal, A. Almohammedi, V. Gupta, Effect of traps on the charge transport in semiconducting polymer PCDTBT. Solid State Electron. **145**, 49–53 (2018)

45. Seema Morab, Manickam Minakshi Sundaram and Almantas Pivrikas, Influence of Traps and Lorentz Force on Charge Transport in Organic Semiconductors, Materials 2023, 16(13), 4691, Sachnik, O., Tan, X., Dou, D. et al. Elimination of charge-carrier trapping by molecular design. Nat. Mater. (2023).

46. J. Zhou, D. He, Y. Li, F. Huang, J. Zhang, C. Zhang, Y. Yuan, Y. Lin, C. Wang, F. Zhao, Reducing trap density in organic solar cells via extending the fused ring donor unit of an A-D–A–Type nonfullerene acceptor for over 17% efficiency. Adv. Mater. **35**(3), 2207336 (2023)

47. Sachnik, O., Tan, X., Dou, D. et al. Elimination of charge-carrier trapping by molecular design. Nat. Mater. (2023).

48. R. Sharma, S. Bhalerao, D. Gupta, Effect of incorporation of CdS NPs on performance of PTB7: PCBM organic solar cells. Org. Electron. **33**, 274–280 (2016)

49. L.Y. Lu, T. Xu, W. Chen, J.M. Lee, Z.Q. Luo, I.H. Jung, H.I. Park, S.O. Kim, L.P. Yu, The role of N-doped multiwall carbon nanotubes in achieving highly efficient polymer bulk heterojunction solar cells. Nano Lett. **13**, 2365–2369 (2013)

50. M.T. Khan, R. Bhargav, A. Kaur, S.K. Dhawan, S. Chand, Effect of cadmium sulphide quantum dot processing and post thermal annealing on P3HT/PCBM photovoltaic device. Thin Solid Films **519**, 1007 (2010)

51. M.T. Khan, A. Kaur, S.K. Dhawan, S. Chand, In-situ growth of cadmium telluride nanocrystals in poly (3-hexylthiophene) matrix for photovoltaic application. J. Appl. Phys. **110**, 044509 (2011)

52. S. Salem Babkair, A. Azam, K. Singh, S.K. Dhawan, M.T. Khan, Synthesis and optoelectrical properties of f-graphene/cadmium selenide hybrid system. J. Nanophoton. **9**, 0930148 (2015)

53. F. Khan, M.T. Khan, S. Rehman, F. Al-Sulaiman, Analysis of electrical parameters of p-i-n perovskites solar cells during passivation via N-doped graphene quantum dots. Surf. Interfaces **31**, 102066 (2022)

54. M.T. Khan, F. Khan, Enhancement in photovoltaic performance of perovskites solar cells through modifying the electron transport layer with reduced graphene oxide. Mater. Lett. **323**, 132578 (2022)

55. S.H. Alrefaee, H.A. Ahmed, M.T. Khan, K.A. Al-Ola, H. Al-Refai, M.A. El-Atawy, New self-organizing optical materials and induced polymorphic phases of their mixtures targeted for energy investigations. Polymers **14**(3), 456 (2022)

56. D.W. Gehrig, I.A. Howard, F. Laquai, Charge carrier generation followed by triplet state formation, annihilation, and carrier recreation in PBDTTT-C/PC60BM photovoltaic blends. J. Phys. Chem. C **119**(24), 13509–13515 (2015)

57. M.T. Khan, A. Almohammedi, M. Shkir, S.W. Aboud, Effect of Ag_2S nanoparticles on optical, photophysical and electrical properties of P3HT thin films. Luminescence **36**(3), 761–768 (2021)

58. A.R. Forouhi, I. Bloomer, Optical dispersion relations for amorphous semiconductors and amorphous dielectrics. Phys. Rev. B **34**(10), 7018–7026 (1986)

59. G.E. Jellison Jr., F.A. Modine, Parameterization of the optical functions of amorphous materials in the interband region. Appl. Phys. Lett. **69**(3), 371–373 (1996)

60. A. Almohammedi, M.T. Khan, M. Benghanem, S. Aboud, M. Shakir, S. Alfaify, Elucidating the impact of PbI2 on photophysical and electrical properties of poly(3-hexythiophene). Mater. Sci. Semicond. Process. **120**, 105272 (2020)

61. M. Taukeer Khan, M. Shkir, B. Alhouri, A. Almohammedi, Y.A.M. Ismail, Modulation of optical, photophysical and electrical properties of poly(3-hexylthiophene) via Gd:CdS nanoparticles. Optik **260**, 169092 (2022)

62. M. Shakir, M.T. Khan, A. Almohammedi, B. Ul Haq, I. Yahia, P.S. Patil, S. Alfaify, S.R. Maidur, V. Ganesh, Influence of Dy doping on key linear, nonlinear and optical limiting characteristics of SnO2 films for optoelectronic and laser applications. Opt. Laser Technol. **108**, 609–618 (2008)

63. G. Li, W.-H. Chan, Y. Yang, Low-bandgap conjugated polymers enabling solution-processable tandem solar cells. Nat. Rev. Mater. **2**, 17043 (2017)

64. F. Bencheikh, D. Duche, C.M. Ruiz, J.-J. Simon, L. Escoubas, Study of Optical properties and molecular aggregation of conjugated low band gap copolymers: PTB7 and PTB7-Th. J. Phys. Chem. C **119**, 24643–24648 (2015)

65. T. Basel, U. Huynh, T. Zheng, T. Xu, L. Yu, Z.V. Vardeny, Optical, Electrical, and magnetic studies of organic solar cells based on low bandgap copolymer with spin ½ radical additives. Adv. Funct. Mater. **25**(12), 1895–1902 (2015)

66. J.A. Guerra, A. Tejada, L. Korte, L. Kegelmann, J.A. Töflinger, S. Albrecht, B. Rech, R. Weingärtner, Determination of the complex refractive index and optical bandgap of CH3NH3PbI3 thin films. J. Appl. Phys. **121**, 173104 (2017)

67. V.S. Vinila, Isac. Jayakumari, Analysis of Bandgap energy and refractive index of ferroelectric perovskite Pbbatio3. Int. J. Eng. Sci. Invent. (IJESI) **7**(8), 40–47 (2018)

68. K. C. Kao and W. Hwang, Electrical Transport in Solids (Pergamon, Oxford, 1981)

69. M.T. Khan, A. Kaur, S.K. Dhawan, S. Chand, Hole transport mechanism in organic/inorganic hybrid system based on in-situ grown cadmium telluride nanocrystals in poly (3-hexylthiophene). J. Appl. Phys. **109**, 114509 (2011)

70. M.T. Khan, A. Almohammedi, Effect of CdS nanocrystals on charge transport mechanism in poly(3-hexylthiophene). J. App. Phy. **122**, 075502 (2017)

71. Z. Chiguvare, V. Dyakonov, Trap-limited hole mobility in semiconducting poly(3-hexylthiophene). Phys. Rev. B **70**, 235207 (2004)

72. R. Kerremans, C. Kaiser, W. Li, N. Zarrabi, P. Meredith, A. Armin, The optical constants of solution-processed semiconductors—new challenges with perovskites and non-fullerene acceptors. Adv. Opt. Mater. **8**, 2000319 (2020)

73. W. da Silva, F. Schneider, A. Mohd Yusoff et al., High performance polymer tandem solar cell. Sci. Rep. **5**, 18090 (2015)

74. M.P. Hughes, K.D. Rosenthal, N.A. Ran, M. Seifrid, G.C. Bazan, T.-Q. Nguyen, Determining the dielectric constants of organic photovoltaic materials using impedance spectroscopy. Adv. Funct. Mater. **28**(32), 1801542 (2018)

75. A.J. Campbell, D.D.C. Bradley, D.G. Lidzey, J. Appl. Phys. **82**, 6326 (1997)